Linear stability of high-speed boundary layer flows at varying Prandtl numbers

Ashwin Ramachandran[*], Bijaylakshmi Saikia[†] and Krishnendu Sinha[‡]

Indian Institute of Technology Bombay, Mumbai, Maharashtra, 400 076, India

Rama Govindarajan[§]

TIFR Centre for Interdisciplinary Sciences, Hyderabad, 500075, India

Accurate prediction of laminar to turbulent transition at hypersonic velocities is a challenging task. The high temperature and low pressure encountered in such applications can lead to large variations in physical and transport properties of the gas. This can result in significant changes in the effective Prandtl number. In this paper, we study the physical effects of Prandtl number on the stability of high Mach number boundary layer flows. Prandtl number values in the range of 0.3 to 1.2 are chosen and a temporal linear stability problem is formulated. The resulting eigenvalue problem is solved using Chebyshev spectral collocation method.

We study the effect of Prandtl number on the eigenspectrum for a range of Mach number, Reynolds number and disturbance wave number. It is found that certain combinations of these parameters lead to synchronization between the fast and the slow modes, which can contribute to the peak growth rate. Two types of branching patterns are observed depending on the Prandtl number, where either the fast or the slow mode can be destabilized due to mode-synchronization. The stability diagrams plotted for a range of Reynolds number and wavenumber show a destabilizing role for increasing the Prandtl number, leading to larger regions of instability, and increased growth rates. This also leads to a significant reduction in the critical Reynolds number specifically at intermediate Mach numbers. High-speed flat plate boundary layer flow is thus found to be highly sensitive to slight changes in the Prandtl number.

Keywords: Hypersonic flow, transport property, fast and slow modes, mode-synchronization.

[*]Undergraduate Student, Department of Aerospace Engineering, Indian Institute of Technology Bombay.

[†]Graduate Student, Department of Aerospace Engineering, Indian Institute of Technology Bombay.

[‡]Associate Professor, Department of Aerospace Engineering, Indian Institute of Technology Bombay, and AIAA Senior Member.

[§]Professor, TIFR Centre for Interdisiplinary Sciences, Hyderabad, 500075, India.

I. Introduction

Hypersonic vehicles fly at an extreme range of stagnation enthalpy, and the aero-thermodynamics associated with them involve strong shock waves, viscous shock layers and non-equilibrium thermo-chemistry. These multiple processes can influence laminar to turbulent transition in different ways. A turbulent boundary layer generates much higher friction and heat transfer, by factors of four or higher, to the vehicle surface compared to a laminar boundary layer. Transition location influences the estimation of aero-heating and skin friction drag, which in turn affect heat shield weight and material, vehicle range, and payload capacity. Therefore predicting the location and streamwise extent of transition in a hypersonic boundary layer is important for avoiding overly conservative design margin for thermal protection systems.

The process of transition from the laminar to the turbulent state can be affected by a wide range of factors[1−3]. For instance, the level of free-stream turbulence[4] and entropy disturbances have a large influence in the transition process. Geometric parameters, such as surface curvature[5], angle of attack[6] and nose bluntness[7−8] can also alter the transition location significantly. In addition, boundary conditions imposed on the vehicle surface, for example, cold/adiabatic, smooth/rough, catalytic/non-catalytic can delay or augment the transition process. At hypersonic speeds, high enthalpy of the flow leads to real gas effects, which include vibrational excitation, dissociation, recombination and exchange reactions, followed by ionization of the gas. Depending on the magnitudes of the relaxation time scales with respect to the fluid-residence time, the thermo-chemical state of the gas can be frozen, equilibrium or non-equilibrium. These high-temperature effects alter the physical as well as transport properties of the gas significantly, which can have a major influence on the stability of hypersonic flows.

Extensive work[9−13] has been carried out to determine the effect of thermo-chemistry on the stability of hypersonic boundary layers. In particular, linear stability theory has been used to study the effect of thermo-chemical parameters on the stability of boundary layers at typical hypersonic conditions. Franko *et. al.*[14] consider a flat plate geometry at a Mach number of 10, and investigate the effect of using different chemistry models for thermodynamic, transport and chemical reactions on boundary layer stability. The wall boundary condition is also varied from adiabatic to cold wall to determine its effect on the second mode growth rate. They observe that the differences for linear stability growth rate prediction between two chemistry models are larger than the differences between thermal non-equilibrium, chemical non-equilibrium, and chemical equilibrium calculations. Similarly, Lyttle *et. al.*[15] consider a spherically blunted right circular cone at a Mach number of 13.5. The sensitivity of the second mode growth rate to the variation of constitutive models for reaction rate, specific heat and transport properties are studied. Amongst the different parameters considered, the variation of transport properties is found to have the most dominant effect on stability characteristics.

Transport properties for a high temperature gas include species diffusivity, in addition to viscosity and thermal conductivity. Due to the presence of various thermo-chemical processes, empirical models, such as Blottner's temperature-based curve fit[16] and transport models derived from kinetic theory are routinely used in hypersonic flow calculations. For precise estimation, more complex models based on collision integrals, such as Chapman−Enskog method[17] and Stuckert's model[18] have to be used. Ref.[15] shows that the transport models of Stuckert and Blottner, predict approximately 10% and 25% difference in the magnitude of viscosity and thermal conductivity, respectively, at the peak boundary layer temperature of 2100 K. This difference results in an 8% variation in the peak growth rate prediction of the second mode instability. Similar results are reported for the $M = 10$ flat plate boundary layer in Ref.[14] The linear stability results differ by around 20% in the peak growth of the second mode, when two different transport models (Blottner and Chapman−Enskog method) are used. The frequency where this peak growth rate occurs also shifts by 8%.

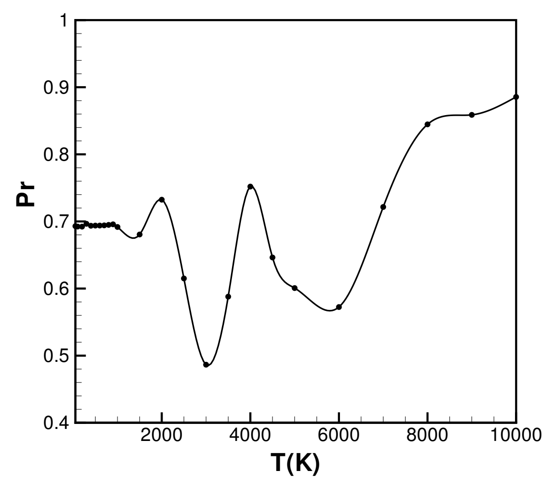

Figure 1. Variation of Prandtl number with temperature at 1 bar pressure (Data taken from Ref.[19]).

The transport properties depend on the internal energy modes and their excitation at elevated temperatures. Different dissociation, ionization and charge-exchange reactions in a high-temperature gas also contribute to the transport property variations. Therefore viscosity and thermal conductivity have different individual variations with temperature and pressure, resulting in large variation in the effective Prandtl number in case of hypersonic flows. Figure 1 shows the variation of Prandtl number for equilibrium air over a range of temperatures at 1 bar pressure. The minimum value of Prandtl number (~ 0.49) is observed at a temperature around 3000 K, while the highest value (~ 0.89) is observed at $10,000$ K.

Previous works[20−22] have extensively studied the physical effect of various parameters such as, Mach number, reference temperature and Reynolds number on boundary layer flow stability. The Prandtl number is mostly fixed, usually at 0.72. In high Mach number flows, however, the effective Prandtl number can vary significantly due to high-temperature effects. This paper is a step towards understanding the physical effect of Prandtl number on the stability of high-speed boundary layer flows. For this, we have considered flat plate boundary layer as the model problem and varied the Prandtl number systematically from 0.3 to 1.2. We intend to carry out a controlled study of the variation of Prandtl number and its effect on flow stability. We therefore neglect thermo-chemical effects, and a perfect gas assumption is used throughout the work. A temporal linear stability is performed and the details of this analysis along with the similarity equations for mean flow are presented in Section II. The stability results are discussed in Section III, followed by the conclusions.

II. Governing equations

A. Base flow

A steady two-dimensional compressible laminar boundary layer flow over a flat plate is solved using the Levy-Lees similarity transformation.[23] In this approach, the coordinates are transformed from the physical domain (x, y) to a transformed space (ξ, η) which are related by,

$$\xi = \int_0^x \rho_e \mu_e u_e dx, \tag{1}$$

$$\eta = \frac{u_e}{\sqrt{2\xi}} \int_0^y \rho dy, \tag{2}$$

where ρ_e, u_e and μ_e are the density, velocity and viscosity at the boundary layer edge. Using the boundary layer approximations along with the above transformation, the Navier Stokes equations reduce to a system of two coupled ODEs given by,

$$(Cf'')' + ff'' = 0 \tag{3}$$

$$\left(\frac{C}{Pr} g'\right)' + fg' + (\gamma - 1) M^2 C f''^2 = 0 \tag{4}$$

where $f' = u^*/u_e$ is the non-dimensional velocity, $g = T^*/T_e$ is the non-dimensional temperature, C is the Chapman-Rubesin factor which is the viscosity-temperature ratio in their non-dimensional forms, M is the edge Mach number, Pr is the local Prandtl number and $\gamma = 1.4$ is assumed. The asterisk and the subscript "e" denote the dimensional and reference quantities respectively, and prime refers to the derivative with respect to the transformed wall normal direction, η. Viscosity is calculated using Sutherland's law, which can be expressed in the non-dimensional form as follows,

$$\mu = T^{\frac{3}{2}} \frac{(1 + B)}{(T + B)}, \tag{5}$$

where $B = 110.4/T_e$ and T_e is in Kelvin. Further, conductivity is calculated assuming a constant value of Pr, based on the free-stream parameters. This constant value of Pr is systematically varied to investigate the effect of variation in Prandtl number on the flow stability.

Eqs. 3 and 4 are subjected to the following boundary conditions at the wall,

$$\text{At } \eta = 0: \;\; f = 0,\, f' = 0,\, g = T_w \;\text{ or }\; g' = 0, \tag{6}$$

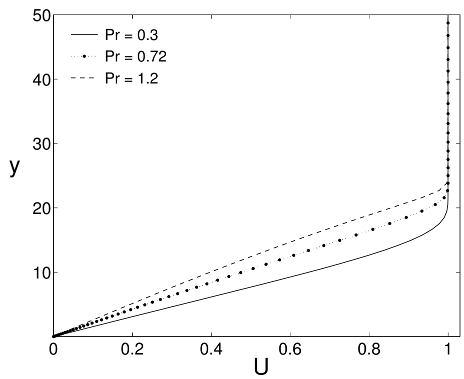

(a) Velocity along the wall-normal direction

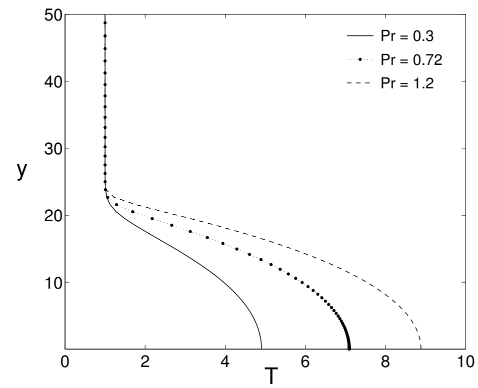

(b) Temperature profile along the wall-normal direction

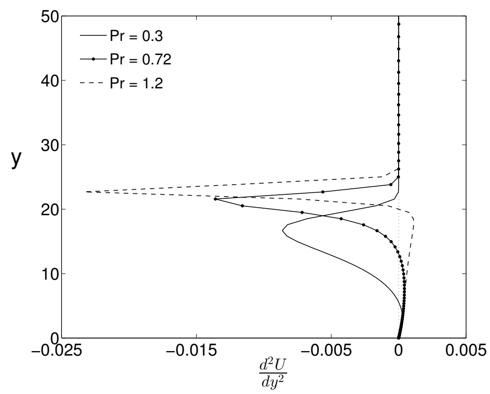

(c) Second derivative of velocity along the wall-normal direction

Figure 2. Effect of Prandtl number on the mean flow at $M = 6$.

where the temperature boundary condition depends on whether the wall is isothermal or adiabatic. Further, at the freestream, the boundary conditions are

$$\text{As } \eta \to \infty : \; f' \to 1, \, g \to 1. \tag{7}$$

In the above equation, ∞ represents boundary layer edge which is characterized by the freestream paratmeters. The base flow (Eqs. 3 and 4) together with the boundary conditions (Eqs. 6 and 7) can be solved as an initial value problem with intial guess values for f'' and g at the wall (for an adiabatic wall considered in the current work). Their actual values can be obtained using the iterative shooting method which ensures that these values satisfy the boundary conditions at the freestream. Note that in order to convert the variable η back to the physical domain y, we use the inverse tranformation given by,

$$\int_0^\eta \sqrt{2}T(\eta)d\eta = \int_0^y \frac{1}{x}\sqrt{Re_x}\,dy \tag{8}$$

The length scale used for the Reynolds number is $\sqrt{\dfrac{x\nu_e}{U_e}}$ and the Mach number specified corresponds to the boundary layer edge Mach number.

The mean velocity and temperature variations for three Prandtl numbers (0.3, 0.72 and 1.2) for $M = 6$ are shown in Figure 2(a) and 2(b). As the Prandtl number is increased, the thickness of the boundary layer increases due to the increase in viscosity (Figure 2(a)). With increase in Pr, the wall temperature also increases significantly, since the recovery factor scales as $\sqrt{Pr}$. The second derivative of velocity is plotted in Figure 2(c) since it is directly related to the calculation of generalized inflection point, and the location of the generalized inflection point plays a key role in the nature of the second mode instabilities. As the Prandtl number is incresed, the location of the inflection point moves away from the wall, which implies that the instabilities are present close to the boundary layer edge for higher Prandtl number cases.

B. Linear Stability

Linear stability equations for the perturbations are derived by representing the instantaneous flow variable (A) as a sum of the mean flow variable $(\bar{A})$ and a small fluctuation quantity $(\tilde{A})$, i.e.,

$$A = \bar{A}\,(y) + \tilde{A}\,(x, y, z, t)\,. \tag{9}$$

Substituting Eq. 9 into the non-dimensional form of the governing equations and neglecting higher-order and non-linear terms, we obtain the linearized perturbation equations.[24] The assumptions employed to derive the linear stability equations are− wavelike disturbance solution, disturbance linearity and parallel mean flow approximation. The fluctuations are expressed in a normal mode form,

$$\tilde{A}\,(x, y, z, t) = \hat{A}\,(y)\, e^{\iota(\alpha x + \beta z - \omega t)}, \tag{10}$$

where $\hat{A}\,(y)$ represents the complex amplitude of the flow variable of a traveling wave with wave number components α, β in the $x - z$ plane and frequency ω. Considering a temporal stability problem with $\omega = kc$ ($k = \sqrt{\alpha^2 + \beta^2}$ and c represents the phase speed of the disturbance wave), where both α, β are real and ω complex, we substitute the perturbed form (Eq. 9) into the linearized disturbance equations. A homogeneous system of ordinary differential equation is thus obtained, which can be expressed as,

$$B\psi = \omega A\psi. \tag{11}$$

Here, $\psi = (\hat{u}, \hat{v}, \hat{w}, \hat{p}, \hat{T})^T$ is the vector of eigenfunctions corresponding to flow velocities, pressure and temperature perturbations. A and B are two $5N \times 5N$ (N is the number of grid points) complex matrices, and its elements are functions of α, β, ω, Re, Pr, M and the mean-flow variables.

Boundary conditions on the perturbations are,

$$\hat{u}\,(0) = \hat{u}\,(\infty) = 0, \quad \hat{v}\,(0) = \hat{v}\,(\infty) = 0, \quad \hat{w}\,(0) = \hat{w}\,(\infty) = 0, \tag{12}$$

$$\hat{T}\,(\infty) = 0, \qquad \frac{d\hat{T}}{d\eta}\,(0) = 0 \;\text{ or }\; \hat{T}\,(0) = 0. \tag{13}$$

We replace the rows corresponding to the boundary conditions on the RHS of Eq. 11 with a multiple of the corresponding rows of B. The corresponding eigenvalues are mapped away from the domain of interest in the eigenvalue plane.The temporal stability problem thus solved, provides the complex frequency $\omega = \omega_r + \iota\omega_i$, where ω_i represents the growth or decay rate of the disturbance wave.

The linear stability equations are solved using the Chebyshev spectral collocation method. The collocation points y_c are given by,

$$y_{c_j} = \cos\frac{\pi j}{N}, \quad j = 0, 1, \ldots N. \tag{14}$$

The domain $\eta = 0$ to $\eta = \eta_{max}$ is mapped to the Chebyshev domain of $y_c \in [-1, 1]$ through the following transformation that accounts for grid stretching:

$$\eta = a\,\frac{1 + y_c}{b - y_c}, \tag{15}$$

where

$$a = \frac{\eta_i \eta_{max}}{\eta_{max} - 2\eta_i}, \;\text{ and }\; b = 1 + \frac{2a}{\eta_{max}} \tag{16}$$

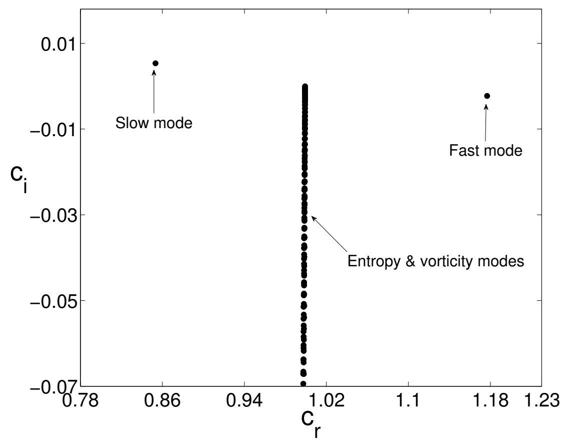

Figure 3. Eigenspectrum plotted for $M = 5$, $Re = 1000$, $\alpha = 0.05$, $\beta = 0$, $Pr = 0.72$ and reference temperature of $300K$.

In the above equation, η_i is a parameter which is used to cluster half of the Chebyshev points below it. The choice of this parameter is made such that there is sufficient clustering within the boundary layer around the point of inflection in the mean velocity.

III. Linear stability results

A. Identification of modes in the eigenspectrum

Figure 3 presents the eigenspectrum computed for a Mach 5 compressible boundary layer flow over a flat plate with two-dimensional disturbances ($\beta = 0$). Reynolds number (Re), Prandtl number (Pr), streamwise wavenumber (α) and the stagnation temperature (T_o) considered for this flow is 1000, 0.72, 0.05 and $300K$ respectively. The spectrum shows the entropy and vorticity modes of the continuous branch near the disturbance phase speed of $c_r = 1$. Two discrete modes are also observed in the range of phase speed considered. The first slow and fast modes are identified from their behaviour at the leading edge of the flat plate as $\alpha \to 0$. The slow discrete mode synchronizes with the slow mode of the continuous spectrum with a phase speed of $1 - \frac{1}{M}$. Similarly, the phase speed of fast discrete mode of the eigenspectrum tends to $1 + \frac{1}{M}$ of fast acoustic wave in the long wavelength limit. As, the wavenumber is increased, the fast discrete mode (F^-) synchronizes with the continuous branch near $c_r = 1$ and departs from the branch as another discrete mode F^+ (Ref.[22]).

B. Validation and sensitivity analysis

Figure 4 shows the sensitivity of the eigenspectrum to the choices of the boundary layer edge location (y_{max}) and the number of Chebyshev points (N) for a $M = 3$, $Pr = 0.7$, $Re = 3000$ and $T_o = 300K$ boundary layer with $\alpha = 0.06$ and $\beta = 0.1$. From Figure 4(a) it can be seen that, an increase in the number of Chebyshev points significantly affects the vorticity/entropy modes that are fast-decaying. It does not alter the acoustic branches of the spectrum much. However, a very low number of points can lead to the vorticity and entropy modes getting closer to the acoustic branch, which in turn leads to spurious interactions between these modes due to low resolution. Therefore, care must be taken to ensure that sufficient number of points are used to avoid such spurious modes. Further, Figure 4(b) shows that the choice of y_{max} affects the higher modes of the two acoustic branches of the spectrum. The fast and slow modes are not affected by the choice of y_{max} beyond a value of 100. However, the location of the higher modes in the acoustic branches can shift depending on y_{max}. A good choice of y_{max} will ensure that the fast and slow modes are accurately captured and that the higher modes do not lead to spurious instabilities.

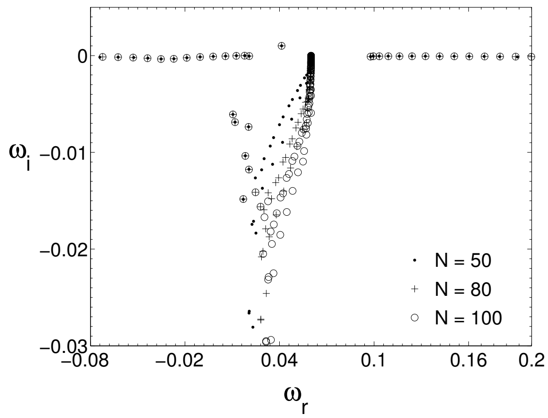

(a) Effect of number of Chebyshev points

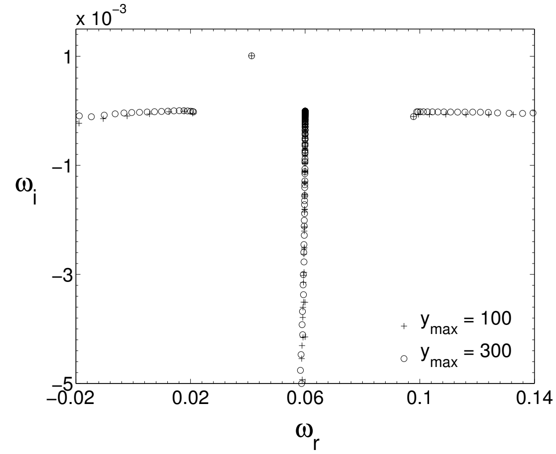

(b) Effect of y_{max}

Figure 4. Sensitivity of the eigenspectrum to the number of points (N), and the location of boundary layer edge (y_{max}) for $M = 3$, $Pr = 0.7$, $Re = 3000$, $\alpha = 0.06$, $\beta = 0.1$ and $T_o = 300K$ boundary layer flow.

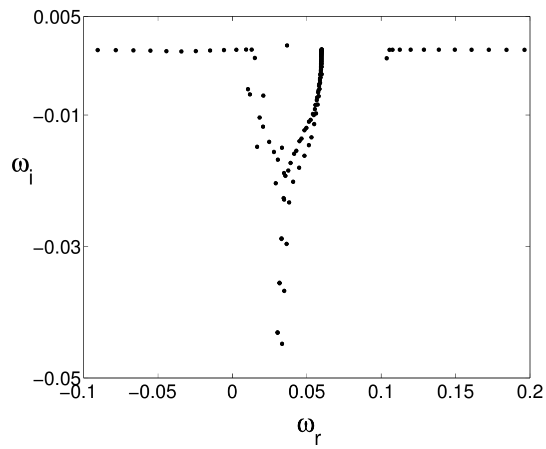

Figure 5. Eigenspectrum plotted for $M = 2.5$, $Re = 3000$, $\alpha = 0.06$, $\beta = 0.1$, $Pr = 0.7$ and reference temperature of $333K$.

In order to validate our code, we compared our results with the test cases mentioned in Ref.,[24] and found a match of the real and imaginary part of the eigenvalues to the fourth and the fifth decimal places respectively (see Table 1). Figure 5 shows the eigenspectrum obtained by our code for the test case corresponding to $M = 2.5$, $Pr = 0.7$, $Re = 3000$ and $T_o = 333K$. The eigenspectrum compares well with that presented in Ref.[25] for the same case.

M	Re	$T_o(K)$	α	β	ω (from Ref.[24])	ω (our code)
0.5	2000	277.78	0.1	0	$0.02908180 + 0.00224419i$	$0.0290679933 + 0.0022429088i$
2.5	3000	333.33	0.06	0.1	$0.0367339 + 0.0005840i$	$0.0367477188 + 0.0005883717i$

Table 1. Comparison of the eigenvalue of the most unstable mode for two test cases mentioned in Ref.[24] at $Pr = 0.7$.

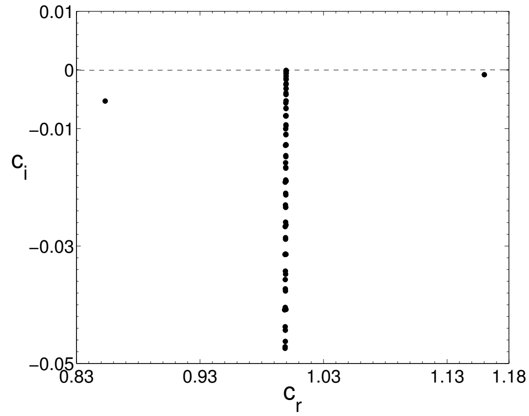

(a) $Pr = 0.3$

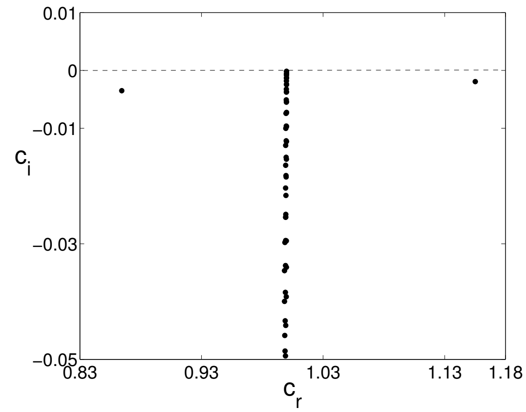

(b) $Pr = 0.72$

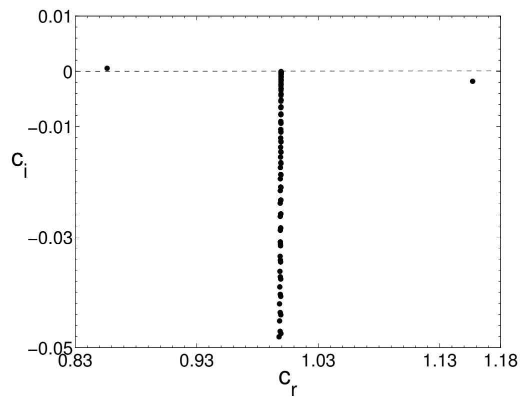

(c) $Pr = 1.2$

Figure 6. Eigenspecta obtained for a flow with $M = 6$, $Re = 2000$, $\alpha = 0.005$, $\beta = 0$, $T_o = 300K$, at varying Prandtl numbers.

C. Effect of Prandtl number on the eigenspectrum

Figure 6 plots the eigenspectra computed for $M = 6$, $Re = 2000$, $\alpha = 0.005$, $\beta = 0$, $T_o = 300$, at three different Prandtl numbers 0.3, 0.72 and 1.2. The first two discrete modes appear in the range of phase speed considered. When Prandtl number is increased from 0.3 to 0.72, the growth rate of the slow mode increases, but the mode is still stable. There is no noticeable effect of Pr change on the fast mode. The effect of Prandtl number on the slow discrete mode is more prominent at $Pr = 1.2$ (Figure 6(c)). The growth rate becomes positive which indicates that the mode has become unstable at higher Prandtl number.

For investigating the effect of Prandtl number on the fast and slow modes, the growth rates of both the modes are plotted in Figure 7, for a flow over a flat plate at $M = 4$ and $Re = 8000$, $\beta = 0$, and reference temperature of $288K$, with three Prandtl numbers. Figure 7(a) shows that increasing the Prandtl number has a significant destabilizing effect on the slow mode. An increase in Pr from 0.65 to 0.8 leads to an increase in the maximum growth rate of the slow mode by a factor of around 10. Further, the destabilizing effect of an increase in Pr is monotonic at each streamwise wavenumber. The wave number corresponding to the peak in the growth rate of the slow mode shifts to higher values at higher Prandtl numbers.

From Figure 7(b), it can be observed that the overall effect of increasing the Prandtl number is also to destabilize the fast mode. This effect is however less pronounced as compared to the slow mode instability. The destabilizing effect of higher Pr is not monotonic for the fast modes. For instance, around a wavenumber of 0.3 and 0.38, it can be seen that the growth rate of the fast mode corresponding to $Pr = 0.65$ is the highest,

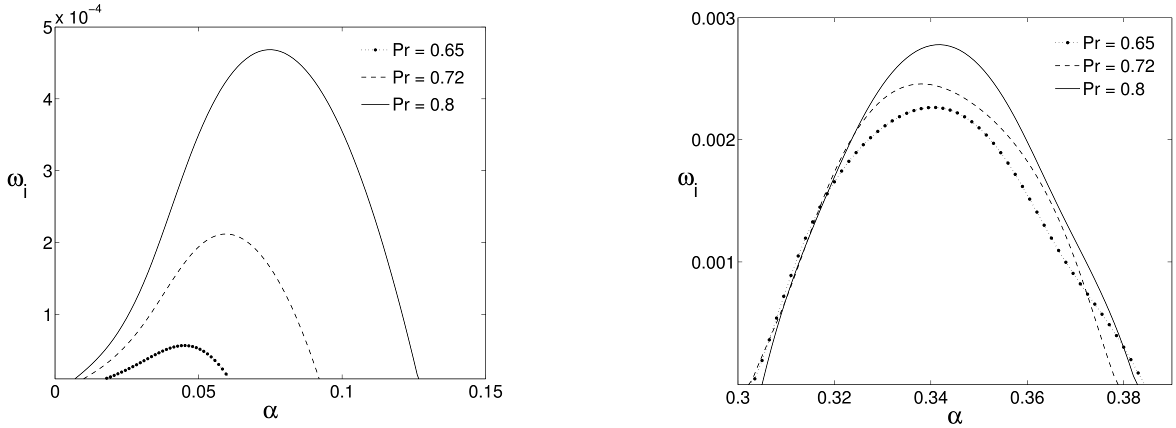

(a) Growth rate of slow mode at different Pr

(b) Growth rate of fast mode at different Pr

Figure 7. Effect of Pr **on the growth rates of the fast and slow modes at** $M = 4$, $Re = 8000$, $\beta = 0$ **and a reference temperature of** $288K$.

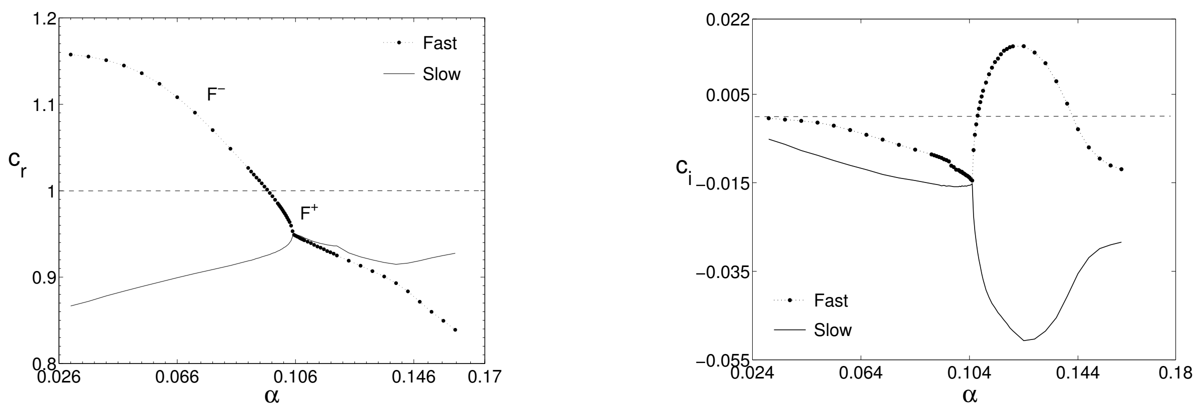

(a) Variation of phase speeds of fast and slow modes with wavenumber at $Pr = 0.37$

(b) Variation of growth rates of fast and slow modes with wavenumber at $Pr = 0.37$

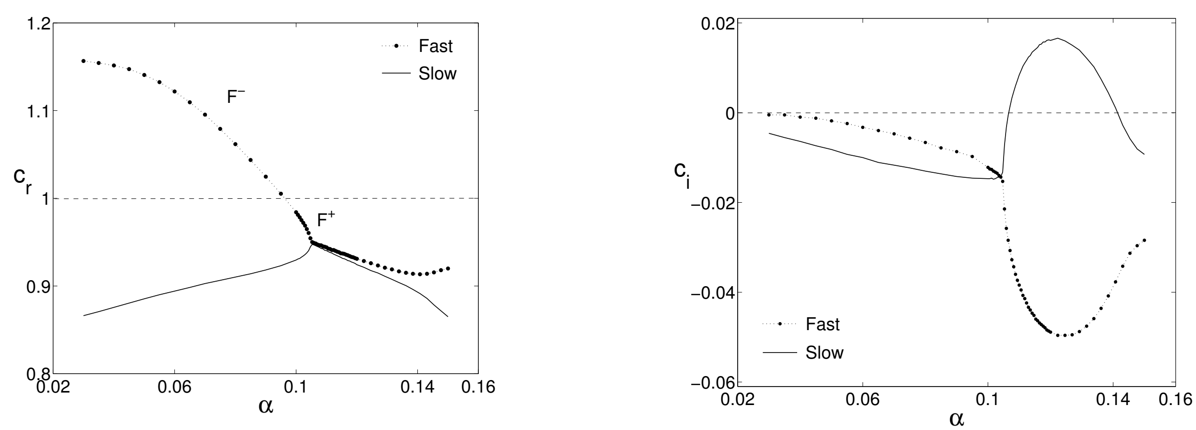

(c) Variation of phase speeds of fast and slow modes with wavenumber at $Pr = 0.38$

(d) Variation of growth rates of fast and slow modes with wavenumber at $Pr = 0.38$

Figure 8. Effect of Prandtl number on the branching pattern at $M = 6$, $Re = 5000$, $T_o = 300K$ **and** $\beta = 0$. **The fast mode after synchronizing with the slow mode becomes the more unstable mode for** $Pr \leq 0.37$, **however for** $Pr \geq 0.38$, **slow mode becomes the most dominant mode after mode-crossing.**

followed by $Pr = 0.72$ and 0.8 respectively. Also, the wave number corresponding to the maximum growth rate does not vary monotonically with changes in Pr, however, the changes in the value of this wave number are small.

D. Branching type depending on the Prandtl number

Figure 8 plots the variation of phase speed and growth rate with wavenumber for the first two discrete modes for a $M = 6$ and $Re = 5000$ compressible flow over a flat plate at a stagnation temperature of $300K$. The wavenumber is varied from around 0.02 to 0.18 for two Prandtl number cases (0.37 and 0.38). When the wavenumber is increased from 0.02, the phase speed of the fast mode decreases monotonically and it synchronizes with the entropy and vorticity modes of the continuous spectrum at a phase speed of around 1 (see Figure 8(a) and 8(c)). Due to this synchronization, a branching of the discrete spectrum is observed and the fast mode i.e., F^- departs from the continuous branch as F^+. The slow mode whose phase speed continuously increases till the synchronization point, synchronizes with F^+ as the wavenumber is increased further. Due to this synchronization, a peak and trough in the growth rates are noticed for the fast and slow modes respectively, as shown in Figure 8(b). However, when the Prandtl number is increased to 0.38, the slow mode which is stable compared to the fast mode before, becomes the most dominant mode after the synchronization with discrete mode F^+ (Figure 8(d)). Therefore depending on the Prandtl number, two different types of branching patterns are observed, where either the slow or the fast mode becomes the most unstable mode. For this case, when the Prandtl number is less than or equal to 0.37, fast mode is the most unstable mode due to synchronization, otherwise slow mode is the most dominant mode starting from a Prandtl number of 0.38. Ref.[22] also reports similar branching pattern for a flat plate boundary layer flow depending on Mach number, but with a constant Prandtl number of 0.72.

E. Eigenfunctions

Figure 9 plots the absolute values of the eigenfunctions for the first two discrete modes along the wall-normal direction for a flat plate flow at $M = 6$, $Re = 3000$, $T_o = 300K$, $\alpha = 0.05$ and $Pr = 0.4$. The eigenfunctions are normalized by the absolute value of pressure perturbation at the wall. The parameters in this case are such that the first two discrete modes are far ahead of the synchronization point and the fast mode is more unstable than the slow mode. Figure 9(a) presents the eigenfunctions for velocity and the viscous sublayer is observed close to the wall for both the modes. The temperature eigenfunctions (Figure 9(b)) shows a peak around a wall normal distance of 16, which is the location of the critical layer for the slow mode. The pressure eigenfunctions are plotted in Figure 9(c) and the slow mode shows a higher magnitude for pressure perturbation compared to the fast mode.

The normalized eigenfunctions for the two fast modes F^- ($c_r = 1 + 0$) and F^+($c_r = 1 - 0$) are presented in Figure 10. The eigenfunctions for both the modes behave similarly in the boundary layer region for all the three eigenfunctions shown here. However, the real parts of the eigenfunctions for velocity and temperature

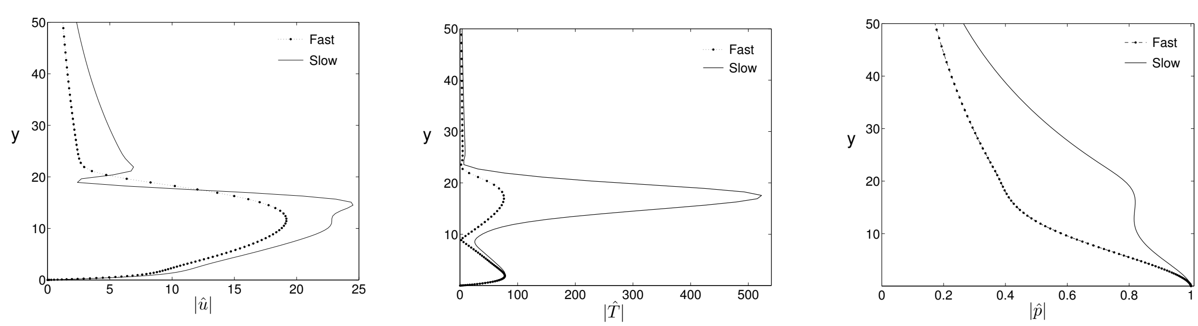

(a) Velocity (b) Temperature (c) Pressure

Figure 9. Eigenfunctions of the slow and fast modes at $M = 6$, $Re = 3000$, $T_o = 300K$, $\alpha = 0.05$, $\beta = 0$ and $Pr = 0.4$.

have large oscillations outside the boundary layer due to the interaction of the fast modes with vorticity and entropy modes of the continuous spectrum, which is also noticed in Ref.[22]

The eigenfunctions for velocity, temperature and pressure in the vicinity of the synchronization point for modes F^+ and slow mode are plotted in Figure 11, at a streamwise wavenumber of 0.1009. We observe an overlap of mode characteristics to a certain extent. However, small differences are observed away from the wall, since the eigenfunctions are not plotted exactly at the branch point.

The eigenfunctions of Figure 12 are plotted at a streamwise wavenumber of 0.122, which corresponds to the maximum growth rate of the slow mode due to the synchronization with F^+. Since the phase speed of both the modes at this wavenumber are close, eigenfunctions of both the modes behave in a similar manner, except near the critical layer which is at a wall-normal distance of around 17.

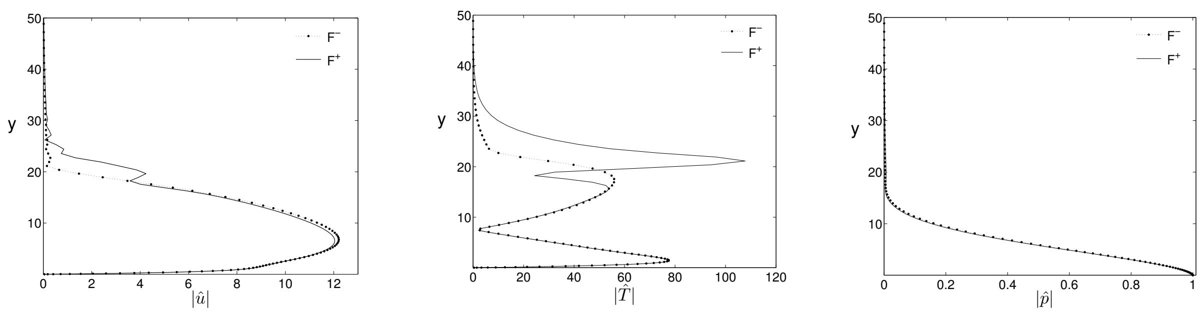

(a) Velocity (b) Temperature (c) Pressure

Figure 10. Eigenfunctions for the fast modes at $M = 6$, $Re = 3000$, $T_o = 300K$, $\beta = 0$ and $Pr = 0.4$. The wavenumbers considered for plotting the eigenfunctions for the modes F^- and F^+ are 0.094 and 0.097 respectively.

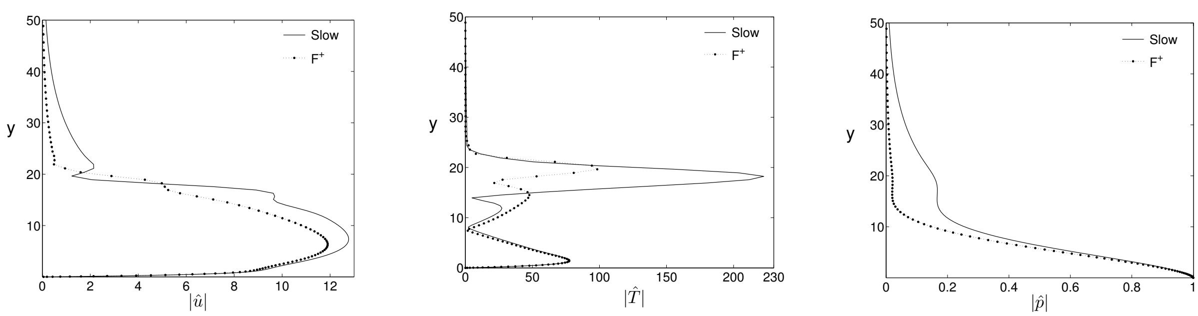

(a) Velocity (b) Temperature (c) Pressure

Figure 11. Eigenfunctions directly before the synchronization (branch point) between the slow and fast mode at $M = 6$, $Re = 3000$, $T_o = 300K$, $\beta = 0$, $Pr = 0.4$ and $\alpha = 0.1009$.

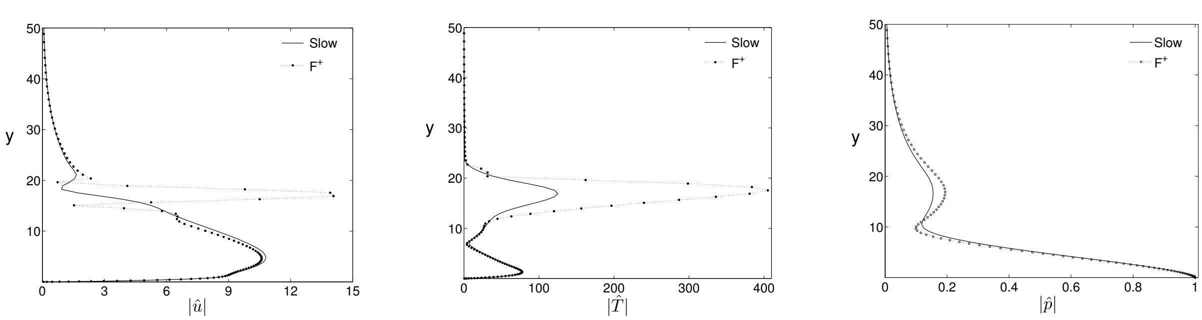

(a) Velocity (b) Temperature (c) Pressure

Figure 12. Eigenfunctions at $\alpha = 0.122$, corresponding to the maximum peak/trough in growth rate during synchronization between the slow and fast mode at $M = 6$, $Re = 3000$, $T_o = 300K$, $\beta = 0$ and $Pr = 0.4$.

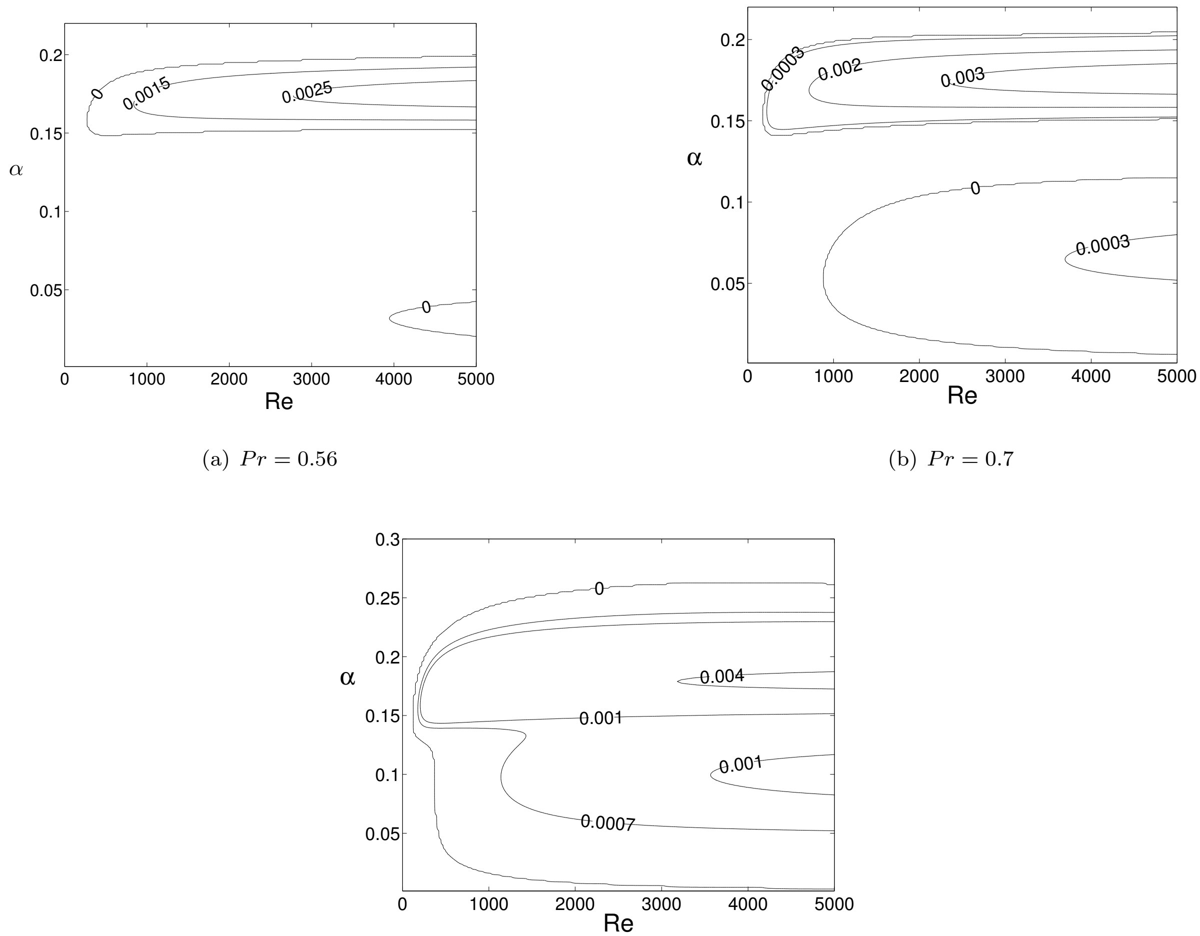

(a) $Pr = 0.56$

(b) $Pr = 0.7$

(c) $Pr = 0.9$

Figure 13. Neutral curves in the $Re - \alpha$ plane for $M = 6$ and different Prandtl numbers.

F. Effect of Prandtl number on the neutral curves in $Re - \alpha$ plane

Figure 13 shows the contours of zero and positive growth rates of the most unstable mode in the $Re - \alpha$ plane for a $M = 6$ boundary layer at different Prandtl numbers with a reference temperature of $288K$. For the Prandtl numbers of 0.56 and 0.7, there are two distinct loops of instability - one occurring at lower wave numbers and the other at higher wave numbers. The lower loop and the upper loop instability are due to the first and second modes respectively.[20−21] At a higher Prandtl number of 0.9, the two loops corresponding to the first and second modes merge to form one large loop of instability. The traces of the two modes can still be seen by noting that there are two loops corresponding to $\omega_i = 0.001$.

Overall, the regions of instability corresponding to both the loops increase with an increase in Prandtl number. It can also be seen that the first mode is strongly destabilized due to an increase in Prandtl number from 0.56 to 0.7, where this loop shifts to much lower Reynolds numbers, resulting in higher growth rates at each Reynolds number with increasing Prandt number. A further destabilizing effect can be seen for this loop when it merges with the second loop for $Pr = 0.9$. The maximum growth rate for the first mode increases by two orders of magnitude, from around 10^{-5} to 10^{-3} when the Pr changes from 0.56 to 0.9 in the Reynolds number range considered.

The effect of Prandtl number on the second mode instability is less pronounced in the sense that the loop characteristics are less affected by a change in Prandtl number. Though the region of instability increases for the second mode when Pr changes from 0.56 to 0.9, the maximum growth rate changes from 0.0025 to 0.004 respectively, where the change is less prominent compared to the first mode instability.

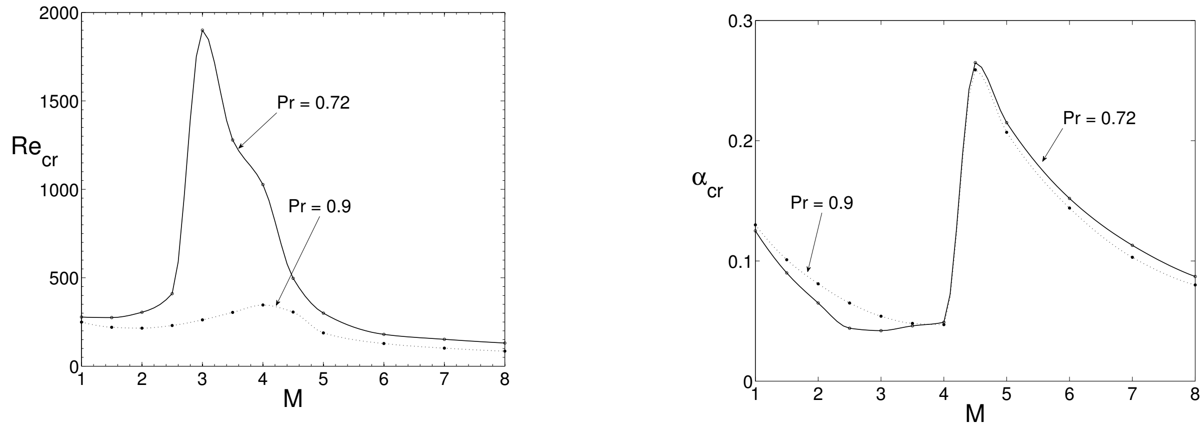

(a) Critical Reynolds number (b) Critical wavenumber

Figure 14. Variation of critical Reynolds number and corresponding wave number with Mach number at two different Prandtl numbers, 0.72 **and** 0.9**.**

Given the ambiguity in the terminology of the first and second modes pointed out in Ref.,[22] we shall also consider the classification the modes as fast and slow, and have a relook at the instability modes in the $Re - \alpha$ plane. For the present case of Mach number of 6 and all the Prandtl numbers considered in Figure 13, both the peaks in growth rate for a fixed Reynolds number correspond to the slow mode instability. So, an increase in the Prandtl number has a destabilizing effect on the slow mode instability, where it is more pronounced in the case of the first instability peak (corresponding to the first mode) at low wavenumber (α).

Note that in the case of $M = 4$ and all the Prandtl numbers presented in Figure 7, the branching pattern is such that the slow and fast modes correspond to the first and second modes respectively. Even in this case, it can be seen that the second mode instability is less affected by the Prandtl number change compared to the first mode instability.

So, we can conclude that the first mode (slow mode) stability is very sensitive to changes in Prandtl number, while the second mode (fast or slow mode depending on the branching pattern) stability is less affected by Prandtl number changes. Note however that an increase in Prandtl number destabilizes both the first and second modes.

G. Effect of Prandtl number on critical Reynolds number and wavenumber

Figure 14(a) shows the variation of the critical Reynolds number and wavenumber with Mach number at two Prandtl numbers of 0.72 and 0.9, and with a reference temperature of $288K$. It can be observed that, the critical Reynolds number decreases significantly as the Prandtl number is increased (Figure 14(a)). This effect is more prominent at intermediate Mach numbers between 2 and 5, where the critical Reynolds number decreases by a factor of around 5 when the Prandtl number changes from 0.72 to 0.9. On the other hand, a further decrease in Prandtl number from 0.72 to 0.6 can lead to an increase in the critical Reynolds number by a factor of around 50 at these intermediate Mach numbers. Further, notice that the variation of critical Reynolds number with Mach number is not monotonic. The critical Reynolds number is maximum at intermediate Mach numbers.

From Figure 14(b), we observe that there is a sharp change in the wavenumber corresponding to the mode leading to the critical Reynolds number between Mach number of 4 and 5. This jump in the critical wave number is due to the change in the most unstable mode, being either the first or the second mode. The first mode is the dominant instability mode at low Mach numbers, while the second mode instability is dominant for higher Mach numbers. Note however that the first mode is always the slow mode, while the second mode could either be the slow or the fast mode depending on the branching pattern. It can be seen that the sudden shift in the critical wave number is less affected by changes in Prandtl number. Also, there are only minor variations in the critical wavenumber with changes in Prandtl number, and the trend is not monotonic with Mach number.

Conclusion

We have investigated the effect of Prandtl number on the stability of high-speed boundary layer flows. Prandtl number values are systematically varied and a temporal linear stability analysis is performed. We find that increasing the Prandtl number has a destabilizing effect on the flow at all Mach and Reynolds numbers. Critical Reynolds number is significantly increased with decrease in Prandtl number especially at intermediate Mach numbers $(2-5)$. Higher growth rates and larger regions of instability are observed in the $Re-\alpha$ stability diagrams as Prandtl number is increased.

Synchronization between the fast and the slow modes often leads to peaks in the growth rates. Depending on the Prandtl number, two types of branching patterns are observed at mode-synchronization, which leads to either the slow or the fast mode becoming the dominant instability. Increasing the Prandtl number destabilizes both the first and the second mode. We observe that the first mode is always the slow mode, while the second mode could either be the slow or the fast mode depending on the branching pattern. Overall, high-speed flat plate boundary layer stability is sensitive to slight changes in Prandtl number.

References

[1] A. Fedorov, "Transition and Stability of High-Speed Boundary Layers," Annual Review of Fluid Mechanics 43, 79 (2011).

[2] X. Zhong and X. Wang, "Direct numerical simulation on the receptivity, instability, and transition of hypersonic boundary layers," Annual Review of Fluid Mechanics 44, 527 (2012).

[3] E. Reshotko, "Hypersonic stability and transition," In Hypersonic Flows for Reentry Problems Vol. 1, ed. By JA Desideri, R Glowinski, J Periaux, Springer: Berlin, 1991, pp. 1834.

[4] S. J. Leib, D. W. Wundrow and M. E. Goldstein, "Effect of free-stream turbulence and other vortical disturbances on a laminar boundary layer," Journal of Fluid Mechanics 380, 169 (1999).

[5] M. R. Malik and D. I. A. Poll, "Effect of curvature on three-dimensional boundary-layer stability," AIAA J. 23 (9), 1362 (1985).

[6] G. G. Mater, "The effect of angle of attack on boundary-layer transition on cones," AIAA J. 10 (8), 1127 (1972).

[7] L. E. Ericsson, "Effect of nose bluntness and cone angle on slender-vehicle transition," AIAA J. 26 (10), 1168 (1988).

[8] M. R. Malik, R. E. Spall, and C. L. Chang, "Effect of nose bluntness on boundary layer stability and transition," AIAA paper No. 1990-0112, 1990.

[9] M. R. Malik and E. C. Anderson, "Real gas effects on hypersonic boundary-layer stability," Physics of Fluids A: Fluid Dynamics 3 (5), 803 (2013).

[10] M. L. Hudson, N. Chokani and G. V. Candler, "Linear Stability of Hypersonic Flow in Thermochemical Nonequilibrium," AIAA J. 35 (6), 958 (1997).

[11] T. W. Robarge and S. P. Schneider, "Laminar Boundary-Layer Instabilities on Hypersonic Cones: Computations for Benchmark Experiments," AIAA Paper No. 2005-5024, 2005.

[12] H. B. Johnson and G. V. Candler, "Thermochemical interactions in the linear stability of hypersonic boundary layers," AIAA Paper No. 98-2438, 1998.

[13] H. B. Johnson, T. G. Seipp and G. V. Candler, "Numerical study of hypersonic reacting boundary layer transition on cones," Physics of Fluids 10 (10), 2676 (1998).

[14] K. J. Franko, R. W. MacCormack and S. K. Lele, "Effects of chemistry modeling on hypersonic boundary layer linear stability prediction," AIAA Paper No. 2010-4601, 2010.

[15] I. J. Lyttle and H. L. Reed, "Sensitivity of second-mode linear stability to constitutive models within hypersonic flow," AIAA Paper No. 2005-889, 2005.

[16] H. Alkandry, I. D. Boyd and A. Martin, "Comparison of Models for Mixture Transport Properties for Numerical Simulations of Ablative Heat-Shields," AIAA Paper 2013-0303, 2013.

[17] B. V. Alexeev, A. Chikhaoui and I. T. Grushin, "Application of the generalized Chapman-Enskog method to the transport-coefficient calculation in a reacting gas mixture," Physical review E 49 (4), 2809 (1994).

[18] G. K. Stuckert, PhD thesis, Dept. of Mechanical and Aerospace Engineering, Arizona State University, Tempe, 1991.

[19] M. Capitelli, G. Colonna, C. Gorse and A. D'Angola, "Transport properties of high temperature air in local thermodynamic equilibrium," The European Physical Journal D-Atomic, Molecular, Optical and Plasma Physics 11 (2), 279 (2000).

[20] L. M. Mack , "Boundary layer stability theoy", Tech. Rep. 709, AGARD, 1984.

[21] S. Ozgen and S. A. Krcal, "Linear stability analysis in compressible, flat-plate boundary-layers," Theoretical and Computational Fluid Dynamics 22 (1), 20 (2008).

[22] A. V. Federov and A. Tumin, "High-speed boundary-layer instability: Old terminology and a new framework," AIAA J. 49 (8), 1647 (2011).

[23] J. D. Anderson Jr., *Hypersonic and high temperature gas dynamics* (McGraw-Hill, USA, 1989), pp. 229-238.

[24] M. R. Malik, "Numerical methods for hypersonic boundary layer stability," Journal of Computational Physics 86 (2), 376 (1990).

[25] A. Hanifi, P. J. Schmid and D. S. Henningson , "Transient growth in compressible boundary layer flow", Physics of Fluids 8 (3), 826 (1996).